Contents lists available at SciVerse ScienceDirect

Physica B

Characterization of quenched-in vacancies in Fe–Al alloys

J. Čížek [a,*], F. Lukáč [a], I. Procházka [a], R. Kužel [a], Y. Jirásková [b], D. Janičkovič [c], W. Anwand [d], G. Brauer [d]

[a] Charles University in Prague, Faculty of Mathematics and Physics, Department of Low Temperature Physics, V Holešovičkách 2, CZ-18000 Praha 8, Czech Republic
[b] Institute of Physics of Materials, Academy of Science of the Czech Republic, Žižkova 513/22, Brno 61662, Czech Republic
[c] Institute of Physics, Slovak Academy of Science, Dúbravská cesta 9, Bratislava 84511, Slovak Republic
[d] Institut für Strahlenphysik, Helmholtz-Zentrum Dresden-Rossendorf, PO Box 510119, Dresden 01314, Germany

ARTICLE INFO

ABSTRACT

Physical and mechanical properties of Fe–Al alloys are strongly influenced by atomic ordering and point defects. In the present work positron lifetime (LT) measurements combined with slow positron implantation spectroscopy (SPIS) were employed for an investigation of quenched-in vacancies in Fe–Al alloys with the Al content ranging from 18 to 49 at.%. The interpretation of positron annihilation data was performed using *ab-initio* theoretical calculations of positron parameters. Quenched-in defects were identified as Fe-vacancies. It was found that the lifetime of positrons trapped at quenched-in defects increases with increasing Al content due to an increasing number of Al atoms surrounding the Fe vacancies. The concentration of quenched-in vacancies strongly increases with increasing Al content from $\approx 10^{-5}$ in $Fe_{82}Al_{18}$ (i.e. the alloy with the lowest Al content studied) up to $\approx 10^{-1}$ in $Fe_{51}Al_{49}$ (i.e. the alloy with the highest Al content studied in this work).

© 2012 Elsevier B.V. All rights reserved.

1. Introduction

Good mechanical strength and excellent oxidation resistance at elevated temperatures make Fe–Al intermetallic alloys very attractive for high temperature applications [1,2]. It is well established that the physical and mechanical properties of Fe–Al alloys are strongly influenced by the atomic ordering and point defects [3].

During cooling from high temperatures Fe–Al alloys with an Al content in the range 30–50 at.% undergo ordering from the disordered A2 phase to the partially ordered B2 structure [4,5]. Fe–Al alloys with lower Al content 22.7–30 at.% undergo also a phase transition from the disordered A2 phase to the partially ordered B2 phase, but ordering continues with decreasing temperature and the B2 structure is transformed into the ordered D0$_3$ phase [4,5].

The structure of all Fe–Al phases is based on two interpenetrating cubic sub-lattices as shown in Fig. 1 and denoted A and B. In the disordered A2 phase both sub-lattices are randomly occupied by Fe and Al atoms. In the partially ordered B2 phase the A sub-lattice is occupied exclusively by Fe atoms, while the B sub-lattice is randomly filled by Fe and Al. Obviously the fraction of Al atoms in the B sub-lattice increases with increasing Al content in the alloy. Finally in the stoichiometric Fe$_{50}$Al$_{50}$ alloy the B sub-lattice is occupied by Al atoms only (while the
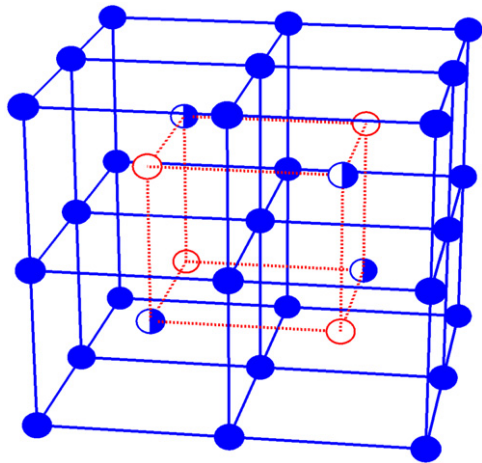
A sub-lattice is filled exclusively by Fe atoms). This structure is called ordered B2 phase. The complex D0$_3$ phase is based on Fe$_3$Al stoichiometry: the A sub-lattice is occupied by Fe atoms only and the B sub-lattice is filled by alternating Fe and Al atoms (see Fig. 1). Obviously a perfect D0$_3$ ordering can be realized only in the stoichiometric Fe$_{75}$Al$_{25}$ alloy. However in Fe–Al alloys the D0$_3$ phase exists in a relatively wide range around the Fe$_{75}$Al$_{25}$ composition and deviations from the stoichiometry are compensated by vacancies or antisite atoms, i.e. Fe or Al atoms located at "wrong" sub-lattice sites.

It was shown that a high concentration of vacancies formed in Fe–Al alloys at high temperatures can be relatively easy quenched down to room temperature [6–8]. In alloys with an Al content close to the stoichiometric Fe$_{50}$Al$_{50}$ composition the concentration of quenched-in vacancies may be as high as several atomic percent [6–8]. Theoretical investigations [9–11] performed for the B2 phase came to the general conclusion that the enthalpy of vacancy formation in the B sub-lattice is significantly higher than in the A sub-lattice. Thus, thermal vacancies in the B2 phase should be Fe-vacancies located in the A sub-lattice. This theoretical prediction was confirmed by coincidence Doppler broadening spectroscopy [12–14].

It was convincingly demonstrated that the hardness of Fe–Al alloys can be increased by quenched-in vacancies [7,15]. Thus, the investigation of vacancies is very important for understanding the physical properties of Fe–Al alloys.

Positron annihilation spectroscopy (PAS) is a non-destructive technique with a high sensitivity to open volume defects

---

* Corresponding author. Tel.: +420 2 2191 2788; fax: +420 2 2191 2567.
E-mail address: Jakub.Cizek@mff.cuni.cz (J. Čížek).

Fig. 1. The structure of the Fe–Al phases. Solid (blue) and dashed (red) lines show the A and B sub-lattices, respectively. In the disordered A2 phase the A and B sub-lattices are randomly occupied by Fe and Al atoms. In the partially ordered B2 phase the A sub-lattice is occupied exclusively by Fe atoms (full blue circles), while the B sub-lattice is filled randomly with Fe and Al atoms. The complex $D0_3$ structure consists of the A sub-lattice occupied by Fe atoms only (full blue circles) and the B sub-lattice consisting of alternating Fe (half filled blue circles) and Al (open red circles) atoms. (For interpretation of the references to color in this figure legend, the reader is referred to the web version of this article.)

e.g. vacancies, di-vacancies, vacancy clusters, etc. [16,17]. PAS involves several experimental techniques; among them positron lifetime (LT) spectroscopy [17] and slow positron implantation spectroscopy (SPIS) [18] are suitable for a determination of the vacancy concentration in Fe–Al alloys. Moreover, a proper inter-pretation of PAS results can be performed with the aid of *ab-initio* theoretical calculations [19] which enable to link experimental data directly with theoretical models. Due to these reasons PAS represents a unique tool for the investigation of vacancies in Fe–Al alloys.

LT spectroscopy was employed most frequently for the investi-gation of vacancies in Fe–Al alloys [12,14,20–23,24–30,32]. High temperature *in situ* LT investigations of Fe–Al alloys enable to determine the vacancy formation enthalpy H_v^f. Würschum et al. [21] found that H_v^f decreases with increasing Al content. However due to the necessity to adapt the LT spectrometer for measurements at high temperatures the achieved time resolution is usually poorer and also the total statistic in LT spectrum is lower than at room temperature measurements. This allowed only for an analysis using the mean positron lifetime [20,21,27,32]. Room temperature LT investigations of quenched-in vacancies in Fe–Al alloys were per-formed by many authors [12,14,22,23,25,26,28–30]. An increase in the lifetime of positrons trapped in quenched-in vacancies with increasing Al content was found in the majority of these works. This was interpreted by an attractive interaction of vacancies and an increasing fraction of so called triple defects, i.e. two Fe-vacancies aligned in [1 0 0] direction and associated with an Fe antisite atom [22,30]. However so far a characterization of vacancies has been performed mostly in Fe–Al alloys with an Al content close to the $Fe_{50}Al_{50}$ stoichiometric composition, since these alloys exhibit the highest concentrations of vacancies. Less is known about vacancies in Fe–Al alloys with compositions close to the Fe_3Al stoichiometry.

SPIS investigations of Fe–Al alloys are absent in the literature although this technique is very helpful for an investigation of vacancies in these alloys because it enables to estimate the vacancy concentration in cases when it is so high that the free positron component cannot be resolved in LT spectra (so-called saturated positron trapping). The ability of SPIS technique to determine defect concentration in materials with very high density of defects has been demonstrated by Krause-Rehberg

et al. [31] who successfully employed SPIS for determination of dislocation density in Ni subjected to severe plastic deformation.

In this work we present PAS investigations of quenched-in vacancies in Fe–Al alloys with an Al content in a broad range from 18 to 49 at.%. Quenched-in vacancies were investigated by LT spectroscopy combined with SPIS. This allowed to determine the vacancy concentration in a wide range from a few ppm up to several at.%. Experimental results were interpreted using state-of-art *ab-initio* theoretical calculations of positron observables.

2. Material and methods

Fe–Al alloys were prepared from high purity Fe (99.99%) and Al (99.99%) by arc melting in Ti-gettered Ar atmosphere. A serie of Fe–Al alloys with an Al concentration from 18 to 49 at.% was prepared. As-cast alloys exhibit coarse grains with a mean diameter of a few mm. Specimens for PAS investigations were cut from the as-cast ingots to a size of about $10 \times 10 \times 1$ mm^3, sealed in evacuated quartz ampoules and annealed at 1000 °C for 1 h. Annealing was finished by quenching of the quartz ampoules into water of room temperature.

A $^{22}Na_2CO_3$ positron source with an activity of 1.2 MBq deposited on a 2 μm thick Mylar foil was used for LT studies. The contribution of positron annihilation in the source and covering foils was measured in a well-annealed pure α-iron (the bulk lifetime of 107.0 ± 0.3 ps) and re-calculated for a particular alloy according to a method suggested in Ref. [33]. The source contribution consists of two components with lifetimes of ≈ 368 ps and ≈ 1.5 ns and intensities of 5–6% and ≈ 1%, respec-tively. These components represent the contribution of positrons annihilated in the source itself and in the covering foil.

A high resolution digital spectrometer [34,35] was employed for LT investigations of the alloys studied. The detector part of the digital LT spectrometer is equipped with two Hamamatsu H3378 photomultipliers coupled with BaF_2 scintillators. Detector pulses are sampled in real time by two ultra-fast Acqiris DC211 8 bit digitizers at a sampling frequency of 4 GHz. The digitized pulses are acquired by a PC and analysis of sampled waveforms is carried out off-line by software using a new algorithm for integral constant fraction timing [36]. The time resolution of the digital LT spectrometer was 145 ps (full width at half maximum (FWHM), ^{22}Na). At least 10^7 annihilation events were accumu-lated in each LT spectrum. Decomposition of LT spectra into exponential components was performed by a maximum-like-lihood code described in Ref. [37].

The SPIS measurements were performed using a magnetically guided variable energy slow positron beam "SPONSOR" [38]. Positron energies were selected so that they covered the region from 0.03 to 35 keV. The diameter of the beam spot was ≈ 4 mm for all positron energies. Energy spectra of annihilation γ rays were measured with a HPGe detector having an efficiency of ≈ 30% and an energy resolution (FWHM) of (1.06 ± 0.01)keV at 511 keV. The Doppler broadening of annihilation profile was evaluated using the line shape S-parameter [16]. All S-parameters shown in this work were normalized to the bulk S-parameter $S_0 = 0.5085(5)$ measured in an $Fe_{75}Al_{25}$ alloy at a positron energy of 35 keV. The dependence of the S-parameter on the positron energy for each alloy was analyzed using the VEPFIT code [39].

X-ray diffraction (XRD) studies were performed on X'Pert Pro diffractometer using Cu-K_α radiation.

3. Theoretical calculations

Theoretical calculations of the positron lifetimes were performed within the so-called standard scheme employing the atomic

superposition (ATSUP) method [41,42]. The electron-positron corre-lations were treated according to Boroński and Nieminen [43]. The lattice parameters used in these calculations were taken from Ref. [44].

Calculations for vacancies were performed using a supercell approach, considering 1024 atom-based supercells. Monovacan-cies were created by removing single atoms from the supercell. The disordered A2 and partially disordered B2 structures were modeled by random filling of the atomic positions in both sub-lattices and in the B sub-lattice, respectively, keeping the total composition in the supercell equal to the alloy composition. Ten independent calculations were performed for each concentration and the arithmetic average of calculated positron lifetimes was used. The variance of the positron lifetime due to atomic disorder was estimated from the spread of calculated results.

4. Results and discussion

XRD investigations revealed that quenched alloys with an Al concentration $c_{Al} \geq 30$ at.% exhibit B2 structure, while those with $18 \leq c_{Al} \leq 30$ at.% exhibit predominantly the disordered A2 phase. This testifies that quenching was fast enough to prevent atomic ordering during cooling.

Fig. 2 shows positron lifetimes of exponential components resolved in the LT spectra of quenched alloys plotted as a function of the Al concentration c_{Al}. LT spectra of alloys with $c_{Al} < 26$ at% were decomposed into two exponential components: the short lived component with lifetime τ_1 represents a contribution of free positrons, while the longer component with lifetime τ_2 comes from positrons trapped at quenched-in vacancies. The relative intensity I_2 of the contribution of positrons trapped at quenched-in vacancies is plotted in Fig. 3 as a function of the Al content. The intensity of positrons trapped at vacancies strongly increases with increasing Al content. In alloys with $c_{Al} \geq 26$ at.% vacancy con-centration becomes so high that the free component cannot be resolved in LT anymore (saturated trapping) and LT spectra are well described by a single component (still denoted by index 2) originating from positrons trapped at vacancies. This is in reason-able agreement with results published by de Diego et al. [22] who
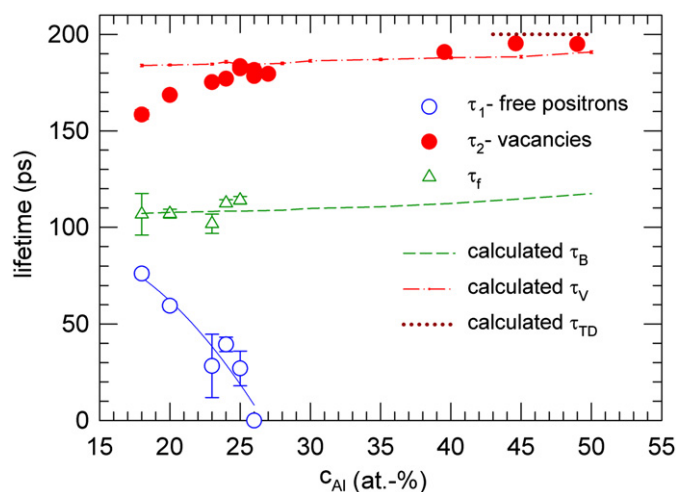

Fig. 3. Relative intensity I_2 of the component with lifetime τ_2 representing positrons trapped at vacancies plotted as a function of the Al concentration c_{Al}.

observed saturated positron trapping in alloys with $c_{Al} \geq 25$ at.% in water-quenched samples and $c_{Al} \geq 30$ at.% in air-quenched samples.

One can see in Fig. 2 that the lifetime of positrons trapped at vacancies increases with increasing Al content. The lifetime τ_V of positrons trapped in vacancies in the A sub-lattice obtained from *ab-initio* theoretical calculations is plotted in Fig. 2 by a dash-dotted line. A good agreement of experimental data with the calculated lifetime τ_V can be seen in alloys with Al content $c_{Al} \geq 25$ at.%. Note that in alloys with an Al content approaching the stoichiometric $Fe_{50}Al_{50}$ composition the concentration of Fe-vacancies in the A sub-lattice becomes extremely high and an attractive interaction of these vacancies leads to the formation of triple defects consisting of two Fe-vacancies in the A sub-lattice aligned in the $\langle 100 \rangle$ direction associated with an antisite Fe atom in the B sub-lattice [10,11]. The calculated lifetime τ_{TD} of positrons trapped in triple defects is plotted in Fig. 2 by a dotted line. Since the experimental lifetimes τ_2 for alloys with high Al content $c_{Al} > 40$ at.% fall somewhere between the calculated lifetime for an Fe-vacancy ($\tau_V \approx 191$ ps) and that for a triple defect ($\tau_{TD} \approx 200$ ps) we can conclude that quenched alloys with high Al content contain most probably a mixture of Fe-vacancies and triple defects.

In alloys with $c_{Al} < 25$ at.% the experimental lifetime τ_2 is lower that the calculated lifetime τ_V. This is most probably due to an inward relaxation of atoms surrounding the vacancy which was not taken into account in theoretical calculations; for a detailed discussion see Ref. [14]. Theoretical calculations revealed an attractive interaction existing between an Al atom (in the B sub-lattice) and a vacancy in the A sub-lattice [45]. This leads to a significant inward relaxation of Al atom towards a vacancy in alloys with low Al content where vacancies are surrounded by one or two Al atoms only. In Fe–Al alloys with higher Al content the number of Al atoms surrounding a vacancy increases and the inward relaxation is canceled due to a repulsive Al–Al interaction.

To put our results into context of data existing in the literature Fig. 4 collects all data of lifetime τ_2 available so far. From inspection of Fig. 4 we can conclude that results of high temperature *in situ* LT studies are in very reasonable agreement with room temperature LT investigations of quenched samples. All data in Fig. 4 consistently show an increase of lifetime of positrons trapped at vacancies with increasing Al content. Theoretical calculations confirmed that the lifetime of trapped positrons increases due to an increasing number of Al atoms surrounding vacancies [46]. Moreover, in alloys with

Fig. 2. Positron lifetimes τ_1 (open circles) and τ_2 (filled circles) of exponential components resolved in LT spectra of quenched alloys plotted as a function of Al concentration c_{Al}. The quantity τ_f calculated using Eq. (1) is plotted in the figure by open triangles. The results of *ab-inito* theoretical calculations are plotted in the figure as well: dashed line, bulk lifetime τ_B of free positrons annihilating in a perfect (defect-free) alloy; dash-dotted line, lifetime τ_V of positrons trapped at vacancies in the A sub-lattice; dotted line, lifetime τ_{TD} of positrons trapped at triple defects.
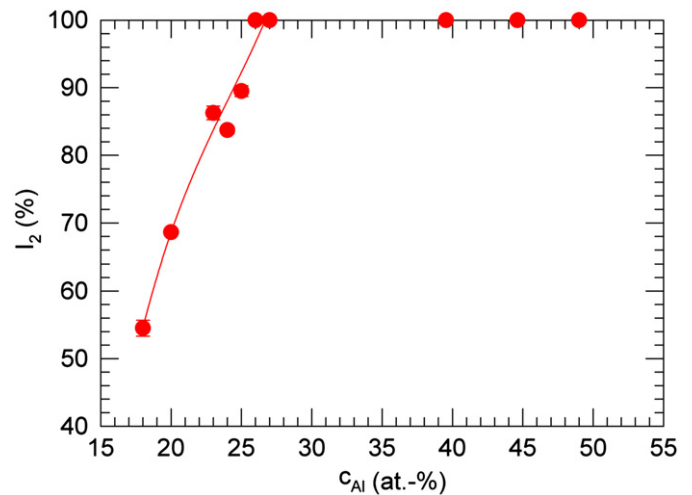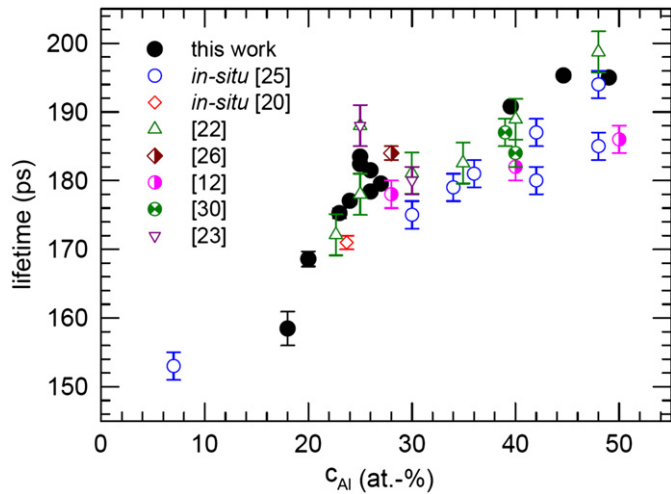
Fig. 4. Dependence of the lifetime τ_2 of positrons trapped at vacancies on Al content c_{Al}. Full circles, this work; open circles, Ref. [24] (in situ LT measurement); open diamonds, Ref. [20] (in situ LT measurement); open triangles (upward), Ref. [22]; half-filled diamonds, Ref. [26]; half-filled circles, Ref. [12]; hourglass circle, Ref. [29]; open triangles (downward), Ref. [23].

high Al content ($c_{Al} > 40$ at.%) the lifetime of trapped positrons increases also due to an increasing fraction of triple defects.

If the free positron component was resolved in a LT spectrum the quantity

$$\tau_f = \left(\frac{I_1}{\tau_1} + \frac{I_2}{\tau_2}\right)^{-1} \qquad (1)$$

can be used to check consistency of the spectrum decomposition with the two state simple trapping model (STM) [17]. If assumptions of the two state STM are fulfilled, i.e. the sample contains a single type of homogeneously distributed positron traps, no detrapping occurs and only thermalized positrons are trapped, then the quantity τ_f equals the bulk positron lifetime τ_B, i.e. the lifetime of free positrons in a perfect (defect-free) material. The quantity τ_f calculated from Eq. (1) is plotted in Fig. 2 (open triangles) together with τ_B obtained from theoretical calculations (dashed line) assuming an A2 structure for alloys with $c_{Al} < 30$ at.% and a B2 structure for alloys with $c_{Al} > 30$ at.% and using lattice parameters determined by Taylor and Jones [44]. One can see in Fig. 2 that the τ_f points are in good agreement with the calculated bulk lifetime curve. This testifies that the assumptions of the two state STM are fulfilled and the concentration of vacancies can be calculated from the expression:

$$c_V = \frac{1}{\nu_V}\frac{I_2}{I_1}\left(\frac{1}{\tau_B} - \frac{1}{\tau_2}\right), \qquad (2)$$

where ν_V is the specific positron trapping rate to vacancies. In this work we used $\nu_V = 4 \times 10^{14}$ s^{-1} reported for vacancies in Fe$_3$Al in Ref. [20]. The concentration of vacancies c_V calculated from Eq. (2) is plotted in Fig. 5.

The free positron component cannot be resolved in a LT spectrum if its relative intensity I_1 falls below $\approx 5\%$. Using Eq. (2) one can calculate that this happens when the concentration of vacancies exceeds 2×10^{-4}. Hence, $c_V \approx 2 \times 10^{-4}$ can be considered as an upper limit of vacancy concentration in Fe–Al alloys which can be determined by LT spectroscopy. In Fe–Al samples studied in this work the saturated positron trapping at vacancies occurs in alloys with $c_{Al} \geq 26$ at.%.

Fig. 6 shows the dependence of the S-parameter on the energy of incident positrons for studied Fe–Al alloys of various composition. At low energies virtually all positrons annihilate at the surface. With increasing energy positrons penetrate deeper and
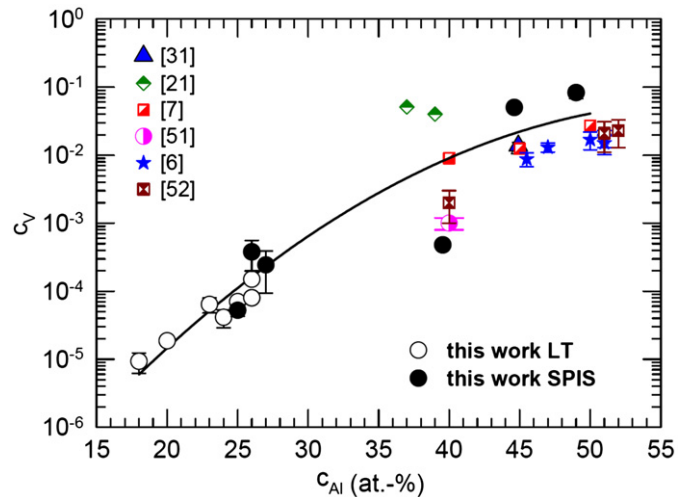
Fig. 5. Concentration of quenched-in vacancies c_V in Fe–Al alloys quenched from 1000 °C. Open circles, c_V determined by LT spectroscopy in this work; full circles, c_V determined by SPIS spectroscopy in this work; filled triangles, c_V obtained by extrapolation of c_V determined in the temperature range 500–800 °C by LT spectroscopy in Ref. [30]; half filled diamonds, c_V calculated using vacancy formation enthalpy and pre-exponential factor determined in the temperature range 390–470 °C by in situ LT spectroscopy in Ref. [21]; half-filled squares, c_V determined from hardness measurements and theoretical modeling by Chang et al. [7]; half filled circles, c_V determined from XRD studies by extrapolation of c_V measured in temperature range 500–950 °C by Joardar et al. [50]; stars, c_V determined from dilatometric measurements combined with XRD [6]; hourglass squares, c_V determined from dilatometric measurements combined with XRD [51].
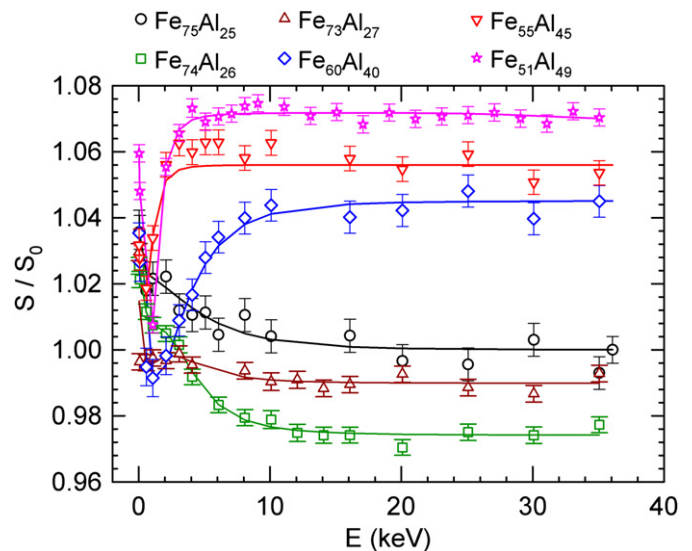
Fig. 6. SPIS results: dependence of the S-parameter on energy E of incident positrons for various quenched alloys. Solid lines show model curves calculated by the VEPFIT software [39].

deeper into the bulk and the fraction of positrons diffusing back to the surface decreases. All Fe–Al samples are covered with a thin oxide layer. The contribution of positrons annihilated inside the oxide layer can be clearly seen in Fig. 6 to be within the energy range 0.5–2.0 keV. At higher energies ($E > 2$ keV) positrons penetrate into the Fe–Al bulk and with increasing energy the S-parameter approaches the bulk value corresponding to the situation when all positrons are annihilated inside the corresponding Fe–Al alloy. Solid lines in Fig. 6 show fitted model curves calculated by VEPFIT software [39] assuming two layered model consisting of (i) a thin oxide surface layer and (ii) a bulk Fe–Al layer. The thickness of the surface oxide layer in various alloys obtained from fitting falls into

the range 15–50 nm. The surface oxide layer contains very high number of defects which is testified by the extremely short positron diffusion length of 4–6 nm. The positron diffusion length L_+ evaluated for every Fe–Al alloy is plotted in Fig. 7. Assuming that quenched Fe–Al alloys contain only a single type of positron traps (quenched-in vacancies), which is confirmed by a single component LT spectrum, the concentration of quenched-in vacancies can be calculated from the formula [40]:

$$c_V = \frac{1}{v_V \tau_B} \left(\frac{L_{+,B}^2}{L_+^2} - 1 \right), \tag{3}$$

where $L_{+,B}$ is the mean positron diffusion length in a perfect (defect-free) alloy. Since $L_{+,B}$ is not known from experiment it was calculated from the expression:

$$L_{+,B} = \sqrt{D_+ \tau_B}, \tag{4}$$

where D_+ is the room temperature positron diffusion coefficient. Experimental data for positron diffusion coefficients are scarce. For aluminum $D_{+,Al} = 1.7 \pm 0.2$ cm^2 s^{-1} was determined by Soininen et al. [48]. For iron only a very rough estimation $D_{+,Fe} > 1$ cm^2 s^{-1} can be found in literature [18]. However positron diffusion coefficients can be determined from semiclassical random walk theory [19,47]:

$$D_+ = \frac{kT}{m^*} \tau, \tag{5}$$

where k is the Boltzmann constant, T is the thermodynamic temperature, $m^* \approx 1.5 m_0$ [18] is the effective positron mass in units of the rest electron mass m_0, and τ is the relaxation time for the scattering process taking place in the material. For metals the acoustic longitudinal phonon scattering dominates and the relaxation time is given by the expression [47]:

$$\tau_{ph} = \sqrt{\frac{8\pi}{9}} \frac{\hbar^4 s}{(m^* kT)^{3/2} \gamma}, \tag{6}$$

where $\hbar$ is the reduced Planck constant, s is the velocity of sound in the material, and γ is the positron-acoustic-phonon coupling constant [19]:

$$\gamma = \frac{E_d}{\sqrt{2\varrho s}}, \tag{7}$$

where ϱ is the mass density and E_d is the deformation potential [47]. The positron diffusion coefficients calculated using this approach for pure Fe and Al are $D_{+,Fe} = 3.8$ cm^2 s^{-1} and $D_{+,Al} = 1.7$ cm^2 s^{-1},
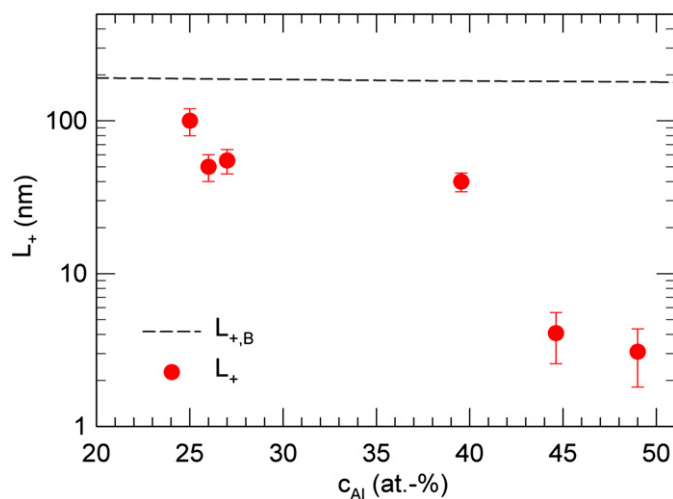
respectively, which is in agreement with available experimental data. Note that for Al we used $E_{d,Al} = -6.7$ eV determined experimentally in Ref. [48], while for Fe we used $E_{d,Fe} \approx -2/3 E_F$ (where E_F is the Fermi energy) [49].

Determination of positron diffusion coefficients D_+ for various Fe–Al alloys requires more demanding calculations which are beyond the scope of this work because the quantities s and E_d are not known. However since D_+ in FeAl alloys decreases with increasing Al content mainly due to decreasing density, in the first approximation it can be estimated by weighted average of positron diffusion coefficients for Fe and Al:

$$D_+ = (1 - c_{Al}) D_{+,Fe} + c_{Al} D_{+,Al}. \tag{8}$$

The positron diffusion length $L_{+,B}$ calculated from Eq. (4) is plotted in Fig. 7 as well.

The concentration of vacancies determined using Eq. (3) is plotted in Fig. 5. One can see in the figure that both LT and SPIS investigations revealed a substantial increase in vacancy concentration with increasing Al content. This indicates that the vacancy formation enthalpy decreases with increasing Al content in concordance with results obtained by Würschum et al. [21]. The concentration of vacancies at 1000 °C calculated from results of LT investigations in Refs. [21,30] is plotted in Fig. 5 as well. Moreover, the vacancy concentration in alloys with high Al content ($c_{Al} > 40$ at.%) becomes so high that it can be detected using differential dilatometry combined with XRD [6,50,51] or through microhardness measurements combined with theoretical modelling [7]. Results of these investigations are also shown in Fig. 5 for comparison with PAS results. One can see in the figure that there is a very reasonable agreement among vacancy concentrations determined using various techniques despite uncertainties implied by necessary approximations and simplifications. The concentration of vacancies increases with increasing Al content roughly by four orders of magnitude from $\sim 10^{-5}$ in an Fe$_{82}$Al$_{18}$ alloy up to $\sim 10^{-1}$ in an Fe$_{50}$Al$_{50}$ alloy.

In cases of short positron diffusion lengths (< 10 nm) the uncertainty of this quantity determined by fitting of $S(E)$ curves measured on our setup falls in the range 1–2 nm. Obviously the positron diffusion length can be reliably determined only if its magnitude is higher than its uncertainty. Hence, the positron diffusion length can be reliably determined by fitting of the $S(E)$ curve if $L_+ > 2$ nm. From Eq. (3) if follows that $L_+ \approx 2$ nm would correspond to an extremely high concentration of vacancies of ≈ 0.2. Obviously such a high concentration of vacancies cannot be reached in any real material. Thus, we can conclude that contrary to LT spectroscopy SPIS is applicable for the determination of the vacancy concentration in almost any practical case and there seems to be no real upper limit for a vacancy concentration which can by determined by this technique. On the other hand, SPIS cannot distinguish between various kinds of defects and the uncertainty of c_V obtained by SPIS is usually larger compared to LT measurements. For these reasons SPIS is suitable mainly for an estimation of the vacancy concentrations in materials with a very high density of defects where LT spectroscopy is not applicable due to saturated positron trapping.

To check whether LT spectroscopy and SPIS gave mutually consistent results, the vacancy concentration in a quenched Fe$_{75}$Al$_{25}$ alloy was determined by both techniques. The concentrations of quenched-in vacancies $c_V = (7.0 \pm 0.5) \times 10^{-5}$ and $(5 \pm 1) \times 10^{-5}$ were obtained from LT and SPIS measurements, respectively. These values are in reasonable agreement taking into account experimental uncertainties.

5. Conclusions

Quenched-in vacancies in Fe–Al alloys with Al concentration from 18 to 49 at.% were investigated in the present work using LT

Fig. 7. The mean positron diffusion length L_+ in Fe–Al obtained from fitting of $S(E)$ curves measured by SPIS. The dashed line shows the calculated positron diffusion length $L_{+,B}$ in a perfect (defect-free) alloy.

spectroscopy combined with SPIS. It was found that the lifetime of positrons trapped in quenched-in vacancies increases with increasing Al concentration. The concentration of quenched-in vacancies c_V was determined using LT and SPIS spectroscopy in alloys with $c_V < 2 \times 10^{-4}$ and using SPIS in alloys with $c_V > 2 \times 10^{-4}$ where the concentration of vacancies is so high that the free positron component cannot be resolved in LT spectra. It was demonstrated that vacancy concentrations estimated by LT and SPIS technique are mutually consistent. The concentration of quenched-in vacancies strongly increases with increasing Al content from 10^{-5} in an $Fe_{82}Al_{18}$ (i.e. the alloy with the lowest Al content studied here) up to 10^{-1} in an $Fe_{51}Al_{49}$. SPIS investigations confirmed an extremely high concentration of vacancies of several at.% estimated previously using XRD, differential dilatometry and microhardness in alloys with a composition approaching the $Fe_{50}Al_{50}$ stoichiometry.

Acknowledgments

References

[1] J.H. Westbrook, Intermetallic Compounds Principles and Practice, vols. 1 and 2, Wiley, Chichester, 1994.
[2] G. Sautho, Intermetallics, WCH, Weinheim, 1995.
[3] J.L. Jordan, S.C. Derbi, Intermetallics 11 (2003) 507.
[4] O. Kubaschewski, Iron-Binary Phase Diagrams, Springer, Berlin, 1982.
[5] T.B. Massalski, Binary Alloy Phase Diagrams, ASM, Metals Park, OH, 1986.
[6] K. Ho, R.A. Dodd, Scripta Metal. 12 (1978) 1055.
[7] Y.A. Chang, L.M. Pike, C.T. Liu, A.R. Bilbrey, D.S. Stone, Intermetallics 1 (1993) 107.
[8] R. Krachler, H. Ipser, B. Sepiol, G. Vogl, Intermetallics 3 (1995) 83.
[9] R. Besson, J. Morillo, Phys. Rev. B 55 (1997) 193.
[10] M. Fähnle, J. Mayer, B. Meyer, Intermetallics 7 (1999) 315.
[11] C.L. Fu, Y.Y. Ye, M.H. Yoo, K.M. Ho, Phys. Rev. B 48 (1993) 6712.
[12] B. Somieski, J.H. Schneibel, L.D. Hulett, Philos. Mag. Lett. 79 (1999) 115.
[13] I.S. Golovin, S.V. Divinski, J. Čížek, I. Procházka, F. Stein, Acta Mater. 53 (2005) 2581.
[14] J. Čížek, F. Lukáč, O. Melikhova, I. Procházka, R. Kužel, Acta Mater. 59 (2011) 4068.
[15] Y. Yang, I. Baker, Intermetallics 6 (1998) 167.
[16] P. Hautojärvi, in: P. Hautojärvi (Ed.), Positrons in Solids, Springer-Verlag, Berlin, 1979, p. 1.
[17] P. Hautojärvi, C. Corbel, in: A. Dupasqier, A. Mills (Eds.), Proceedings of the International School of Physics 'Enrico Fermi', Course CXXV, IOS Press, Varenna, 1995, p. 491.
[18] P.J. Schultz, K.G. Lynn, Rev. Mod. Phys. 60 (1988) 701.
[19] M.J. Puska, R.M. Nieminen, Rev. Mod. Phys. 66 (1994) 841.
[20] H.E. Schaefer, R. Würschum, M. Šob, M. Žák, W. Yu, W. Eckert, F. Banhart, Phys. Rev. B 41 (1990) 11869.
[21] R. Würschum, C. Grupp, H.-E. Schaefer, Phys. Rev. Lett. 75 (1995) 97.
[22] N. de Diego, F. Plazaola, J.A. Jiménez, J. Serna, J. del Río, Acta Mater. 53 (2005) 163.
[23] Y. Ortega, N. de Diego, F. Plazaola, J.A. Jiménez, J. del Río, Intermetallics 15 (2007) 177.
[24] A. Broska, J. Wolff, M. Franz, T. Hehenkamp, Intermetallics 7 (1999) 259.
[25] Y. Jirásková, O. Schneeweiss, M. Šob, I. Novotný, Acta Mater. 45 (1997) 2147.
[26] J. Kansy, A. Hanc, D. Giebel, M. Jabllońska, Acta Phys. Polon. A 113 (2008) 1409.
[27] H.E. Schaefer, B. Damson, M. Weller, E. Arzt, E.P. George, Phys. Status Solidi A 160 (1997) 531.
[28] Y. Jirásková, O. Schneeweiss, M. Šob, I. Novotný, I. Procházka, F. Bečvář, J. Phys. 5 (1995) C1.
[29] S. Gialanella, R.S. Brusa, W. Deng, F. Marino, T. Spataru, G. Principi, J. Alloys Compd. 317-318 (2001) 485.
[30] T. Haraguchi, F. Hori, R. Oshima, M. Kogachi, Intermetallics 9 (2001) 763.
[31] R. Krause-Renberg, V. Bondarenko, E. Thiele, R. Klemm, N. Schell, Nucl. Instrum. Methods B 240 (2005) 719.
[32] J. Wolff, M. Franz, T. Hehenkamp, J. Radioanal. Nucl. Chem. 210 (1996) 591.
[33] H. Surbeck, Helv. Phys. Acta 50 (1977) 705.
[34] F. Bečvář, J. Čížek, I. Procházka, J. Janotová, Nucl. Instrum. Methods A 539 (2005) 372.
[35] F. Bečvář, J. Čížek, I. Procházka, Acta Phys. Polon. A 113 (2008) 1279.
[36] F. Bečvář, Nucl. Instrum. Methods B 261 (2007) 871.
[37] I. Procházka, I. Novotný, F. Bečvář, Mater. Sci. Forum. 255-257 (1997) 772.
[38] W. Anwand, H.-R. Kissener, G. Brauer, Acta Phys. Polon. A 88 (1995) 7.
[39] A. van Veen, H. Schut, M. Clement, J. de Nijs, A. Kruseman, M. IJpma, Appl. Surf. Sci. 85 (1995) 216.
[40] A. van Ween, H. Schut, J. de Vries, R.A. Hakvoort, M.R. Ijpma, in: P.J. Schultz, G.R. Massoumi, P. Simpson (Eds.), AIP Conference Proceedings No. 218, AIP, New York, 1990, p. 83.
[41] M.J. Puska, R.M. Nieminen, J. Phys. F: Met. Phys. 13 (1983) 333.
[42] A.P. Seitsonen, M.J. Puska, R.M. Nieminen, Phys. Rev. B 51 (1995) 14057.
[43] E. Boroński, R.M. Nieminen, Phys. Rev. B 3820 (1986) 34.
[44] A. Taylor, R.M. Jones, J. Phys. Chem. Solids 6 (1958) 16.
[45] H. Amara, C.C. Fu, P. Maugis, Phys. Rev. B 81 (2010) 174101.
[46] O. Melikhova, J. Čížek, J. Kuriplach, I. Procházka, M. Cieslar, W. Anwand, G. Brauer, Intermetallics 18 (2010) 592.
[47] J. Bardeen, W. Shockley, Phys. Rev. B 80 (1950) 72.
[48] E. Soininen, H. Huomo, P.A. Huttunen, J. Mäkinen, P. Hautojärvi, A. Vehanen, Phys. Rev. B 41 (1990) 6227.
[49] B. Bergersen, E. Pajanne, P. Kubica, M.J. Stott, C.H. Hodges, Solid State Commun. 15 (1974) 1377.
[50] J. Joardar, R.Y. Fillit, A. Fraczkiewicz, Philos. Mag. Lett. 85 (2005) 299.
[51] D. Paris, P. Lesbats, J. Phys. Colloq. 38 (1977) C7.